Available online at www.eccomasproceedia.org
Eccomas Proceedia SMART (2023) 1778-1787

ECCOMAS
Proceedia

X ECCOMAS Thematic Conference on Smart Structures and Materials
SMART 2023
D.A. Saravanos, A. Benjeddou, N. Chrysochoidis and T. Theodosiou (Eds)

FEM MODELING OF SMART SELF-BIASED MAGNETOELECTRIC COMPOSITES FOR ENERGY TRANSDUCER APPLICATIONS

T. HUANG[*], H. TALLEB[*], A. GENSBITTEL[*], L. BECERRA[†], Y. ZHENG[†], M. MARANGOLO[†], Z. REN[*]

[*] Sorbonne Université, CNRS, Laboratoire de Génie Electrique et Electronique de Paris, 75252, Paris, France

[*] Université Paris-Saclay, CentraleSupélec, CNRS, Laboratoire de Génie Electrique et Electronique de Paris, 91192, Gif-sur-Yvette, France.

[†] *Sorbonne Université, CNRS, Institut des NanoSciences de Paris, INSP, UMR7588, F-75005 Paris, France*

Abstract. This study suggests using a multiphysics tool based on the Finite Element Method (FEM) to explore two types of magnetoelectric composites (MECs): self-biased MEC Ni/(YXl)163˚ $LiNbO_3$/Ni and non-self-biased Ni/PZT-5H/Ni. The numerical code incorporates the nodal shell element principle to analyze the thin magnetostrictive Ni material (10 µm) and considers its nonlinear behavior using a simplified magnetoelastic anhysteretic model in the FEM formulation.

Key words: Self-biased Magnetoelectric, Multiphysics Problems, FEM, Shell Element, nonlinear magnetoelastic model.

1 INTRODUCTION

Multifunctional magnetoelectric composites (MECs) have become increasingly popular in various fields, including biomedical applications and engineering devices [1]–[3]. These materials consist of piezoelectric and magnetostrictive materials that are indirectly coupled through the elastic phase. In most cases of the direct operated mode, the magnetic excitation is composed of a small dynamic magnetic signal δH_{ac} around a fixed static magnetic bias H_{dc} where the magnetoelectric (ME) response is maximal. In this way, a strong elastic stress is induced within the magnetostrictive material and provides a corresponding strain onto the piezoelectric material, a dynamic electric voltage V is then generated across the electrodes of the piezoelectric material as shown in Figure 1, and the efficiency of the MECs is commonly measured using the magnetoelectric coefficient ($\alpha_E = \delta V/(\delta H_{ac} \cdot t_p)$), where t_p is the thickness of the piezoelectric layer. However, the need for a magnetic bias generated by permanent magnets presents a significant challenge in creating compact and affordable devices. Recent research has focused on self-biased ME materials composed of magnetostrictive layers,

Peer-review under responsibility of the organizing committee of SMART 2023.
doi: 10.7712/150123.9948.444993

such as Ni, which exhibit a remarkable remanent ME response for zero H_{dc}, thereby offering a potential solution to this challenge [4]–[6].

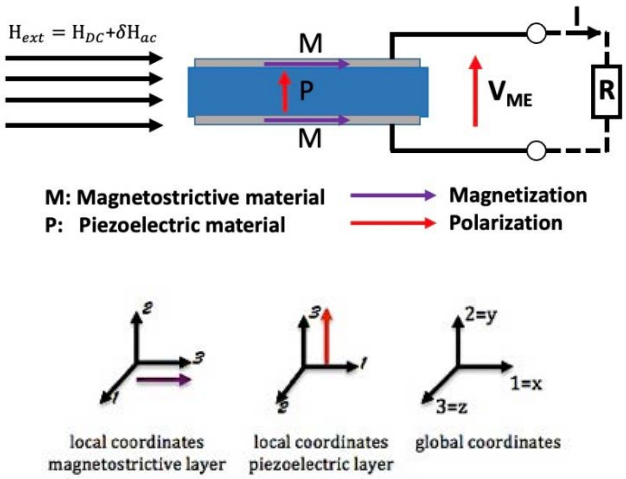

Figure 1: The studied MECs exicited in L-T mode

This paper proposes investigating two different types of MECs, Ni/(YXl)163˚ $LiNbO_3$ (10×5×0.1 mm^3)/Ni and Ni/PZT-5H (11×5×0.22 mm^3)/Ni. The nickel (Ni) films, which are approximately 10 µm thick were deposited using RF sputtering. The study focuses on the ME L-T working mode as shown in Figure 1, where magnetic excitation is applied longitudinally and electric polarization is transversal, using a multiphysics tool based on the Finite Element Method (FEM). The numerical code uses the nodal shell element principle to consider the thin magnetostrictive Ni material and includes its non-linear behavior using a simplified magnetoelastic anhysteretic model in the FEM formulation. To validate the accuracy of the multiphysics tool, the simulation results in both static and dynamic regimes are compared to experimental results.

2 FEM MODELING USING SHELL ELEMENT

2.1 Governing equations

The equilibrium and the compatibility equations for a magnetoelectric problem are respectively given by (1) and (2):

$$\begin{aligned} div\boldsymbol{T} + \boldsymbol{f} &= \rho_v \partial_t^2 \boldsymbol{u} \\ \mathrm{div}\boldsymbol{D} &= \rho \\ \mathrm{curl}\,\boldsymbol{H} &= \boldsymbol{J} \end{aligned} \tag{1}$$

where $\boldsymbol{f}$ is the body force, ρ is the electrical charge and $\boldsymbol{J}$ is the free current density. $\boldsymbol{T}$, $\boldsymbol{D}$ and $\boldsymbol{H}$ represent respectively the mechanical stress tensor, electric displacement field and magnetic field. Finally, $\boldsymbol{u}$, $\boldsymbol{f}$ and ρ_v are respectively the mechanical displacement, the externally applied volume force and the mass density of the medium. In this study, we consider $\rho = 0$ and $\boldsymbol{J} = 0$.

$$\boldsymbol{S} = \frac{1}{2}(grad(\boldsymbol{u}) + grad^{T}(\boldsymbol{u})) \qquad (2)$$
$$\text{curl}\,\boldsymbol{E} = 0$$
$$\text{div}\boldsymbol{B} = 0$$

where $\boldsymbol{S}$, $\boldsymbol{E}$ and $\boldsymbol{B}$ are respectively the mechanical strain, the electric field and the magnetic induction.

The coupled constitutive equations for a ME problem, which combine piezomagnetic and piezoelectric couplings can be written as follows:

$$\begin{bmatrix} \boldsymbol{T} \\ \boldsymbol{D} \\ \boldsymbol{H} \end{bmatrix} = \begin{bmatrix} (\mathbb{c}^{\boldsymbol{E}} + \mathbb{c}^{\boldsymbol{B}}) & -\mathbb{e}^{\mathbf{T}} & -\mathbb{h}^{\mathbf{T}} \\ -\mathbb{e} & \mathbb{p}^{S} & 0 \\ -\mathbb{h} & 0 & \mathbb{v}^{S} \end{bmatrix} \begin{bmatrix} \boldsymbol{S} \\ \boldsymbol{E} \\ \boldsymbol{B} \end{bmatrix} \qquad (3)$$

Here, the symmetric tensors $\mathbb{e}$ and $\mathbb{h}$ contain the piezoelectric and piezomagnetic material coefficients, respectively. The diagonal elements $\mathbb{c}^{\boldsymbol{E}}$ and $\mathbb{c}^{\boldsymbol{B}}$ represent the stiffness tensors of piezoelectric and magnetostrictive elements under constant electric field and constant magnetic induction, respectively. The $\mathbb{p}^{S}$ and $\mathbb{v}^{S}$ are the permittivity under constant strain and the reluctivity under constant strain, respectively.

Once the coupled magnetoelectric problem with a 2D assumption [7]–[9] has been discretized into finite elements, the unknown variables of the problem consist of the mechanical displacement $\boldsymbol{u} = \{u_x, u_y\}$, the electric potential V, and the z-component of the magnetic potential a_z at the mesh nodes. The fields $\boldsymbol{S}$, $\boldsymbol{E}$ and $\boldsymbol{B}$ are then expressed in matrix form using the derivatives of the nodal shape functions $N_{u,v,a}$.

$$\begin{bmatrix} \boldsymbol{S} \\ \boldsymbol{E} \\ \boldsymbol{B} \end{bmatrix} = \begin{bmatrix} \mathrm{G_u} & 0 & 0 \\ 0 & \mathrm{G_v} & 0 \\ 0 & 0 & \mathrm{G_a} \end{bmatrix} \begin{bmatrix} \boldsymbol{u} \\ V \\ a_z \end{bmatrix} \qquad (4)$$

where $\mathrm{G_u} = \frac{1}{2}\left(grad_{\mathrm{xy}} + grad_{\mathrm{xy}}{}^{\mathrm{T}}\right)[N_u] = D[N_u]$, $\mathrm{G_V} = \mathrm{grad_{xy}}[N_v]$, $\mathrm{G_a} = \mathrm{r}^{*} grad_{\mathrm{xy}}[N_a]$ are gradient operators with $r^{*} = [0 \quad 1, -1 \quad 0]^{\mathrm{T}}$ a rotation matrix in Cartesian coordinates.

2.2 Modeling of thin magnetostrictive layer

When MECs are composed of thin layers and thick layers [10], the thickness of the magnetostrictive layer (δ) is typically much smaller than the dimension of the piezoelectric layer, which includes its thickness (t_p) and length (L_x) (usually δ/A <10^{-3}, where $A = \max(\|t_p\|) \cup \|L_x\|$). Traditional finite element modeling of such structures requires an extremely fine mesh, which can be time-consuming. To simplify this process, an effective thin layer can be considered for the magnetostrictive layer and modeled using a line element [11]. The nodes of the line element are duplicated, as shown in Figure 2, using the gradient approximation proposed in [12] to degenerate the 3-node linear triangular element into a 2-node line element.

$$grad_L[N\emptyset] = \frac{1}{2}\frac{\partial}{\partial x}\left(\sum_{i=1}^{2} N_i^0 \langle \emptyset_i \rangle\right)\overrightarrow{e_x} + \frac{1}{\delta}\left(\sum_{i=1}^{2} N_i^0 [\emptyset_i]\right)\overrightarrow{e_y} \tag{5}$$

where $\langle \emptyset_i \rangle = \emptyset_i^+ + \emptyset_i^-$ and $[\emptyset_i] = \emptyset_i^+ - \emptyset_i^-$ are, respectively, the weighted average and the jump of unknown variable $\emptyset_i$ along and across the thickness δ. The annotations $\emptyset_i^+$ and $\emptyset_i^-$ represent the nodal values of $\emptyset_i$ on both sides of the thin layer element and N_i^0 is the shape function for 2-node line element.

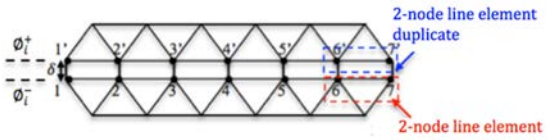

Shell nodal elements introduced in duplicate the 2-node line element

Figure 2: Illustration of the method to consider thin layer.

As a result, we model the effective thin layer using symmetric 4-node elements (Q4 element), which approximate the unknown variables $\boldsymbol{u} = \{u_x, u_y\}$, V, and a_z using shape functions (6) and (7). These functions are obtained by degenerating the 2-node line element.

$$\{\boldsymbol{u}\} = N_{ui}^0 \boldsymbol{u_i}, \{V\} = N_i^0 \boldsymbol{V_i}, \{a_z\} = N_i^0\, a_{z_{\boldsymbol{i}}}$$

with the shape functions

$$N_{ui}^0 = \begin{bmatrix} N_1' & 0 & N_2' & 0 & 0 & 0 & 0 & 0 \\ 0 & N_1' & 0 & N_2' & 0 & 0 & 0 & 0 \\ 0 & 0 & 0 & 0 & N_1' & 0 & N_2' & 0 \\ 0 & 0 & 0 & 0 & 0 & N_1' & 0 & N_2' \end{bmatrix} \tag{6}$$

$$N_i^0 = \begin{bmatrix} N_1' & 0 & N_2' & 0 \\ 0 & N_1' & 0 & N_2' \end{bmatrix} \tag{7}$$

where $N_1' = 1 - \frac{x}{L_e}$, $N_2' = \frac{x}{L_e}$ and L_e denotes the length of the 2-node line element.

The unknown variables are decomposed as:

$$\begin{gathered} \boldsymbol{u_i} = \{u_{x1}^+ \quad u_{y1}^+ \quad u_{x2}^+ \quad u_{y2}^+ \quad u_{x1}^- \quad u_{y1}^- \quad u_{x2}^- \quad u_{y2}^-\}^T \\ \boldsymbol{V_i} = \{V_1^+ \quad V_1^- \quad V_2^+ \quad V_2^-\}^T \\ \boldsymbol{a_i} = \{a_1^+ \quad a_1^- \quad a_2^+ \quad a_2^-\}^T \end{gathered} \tag{8}$$

And the degenerate gradient operators G_u^{shell}, G_V^{shell} and G_a^{shell} are given by:

$$\begin{gathered} G_u^{shell} = D'[N_{ui}^0] \\ G_V^{shell} = G_a^{shell} = grad_L[N_i^0] \end{gathered} \tag{9}$$

with $D' = \begin{bmatrix} \frac{1}{2}\frac{\partial}{\partial x} & 0 & \frac{1}{2}\frac{\partial}{\partial x} & 0 \\ 0 & \frac{1}{\delta} & 0 & -\frac{1}{\delta} \\ \frac{1}{\delta} & \frac{1}{2}\frac{\partial}{\partial x} & -\frac{1}{\delta} & \frac{1}{2}\frac{\partial}{\partial x} \end{bmatrix}$ and $grad_L = \begin{bmatrix} \frac{1}{2}\frac{\partial}{\partial x} & \frac{1}{2}\frac{\partial}{\partial x} \\ \frac{1}{\delta} & -\frac{1}{\delta} \end{bmatrix}$.

2.3 Finite element formulation

After the FEM discretization, the general coupling system equation is expressed as [7]–[9]:

$$[\mathcal{M}]\{\ddot{\mathcal{X}}\} + [\mathcal{C}]\{\dot{\mathcal{X}}\} + [\mathcal{K}]\{\mathcal{X}\} = [\mathcal{F}] \tag{10}$$

where $[\mathcal{K}]$ is the electro-magneto-mechanical stiffness matrix, $[\mathcal{C}]$ the mechanical damping matrix, $[\mathcal{M}]$ the mechanical mass matrix, $\{\mathcal{X}\}$ the unknown vector and $\{\mathcal{F}\}$ the excitation vector. In the case where the linear triangular elements are used, the submatrices in $[\mathcal{K}]$ can be formulated as [7], [8] :

$$\begin{bmatrix} K_{uu} \\ K_{pp} \\ K_{aa} \end{bmatrix} = \sum_e \int_{\Omega_e} \begin{bmatrix} [G_u]^t \mathbb{c} [G_u] \\ [G_p]^t \mathbb{p} [G_p] \\ [G_a]^t \mathbb{v} [G_a] \end{bmatrix} d\Omega \tag{11}$$

and

$$\begin{bmatrix} K_{up} \\ K_{ua} \end{bmatrix} = \sum_e \int_{\Omega_e} \begin{bmatrix} [G_u]^t \mathbb{e}^t [G_p] \\ [G_u]^t \mathbb{g}^t [G_a] \end{bmatrix} d\Omega \tag{12}$$

where $\mathbb{c}$, $\mathbb{p}$, $\mathbb{v}$, $\mathbb{e}$ and $\mathbb{g} = \mathbb{q}\mathbb{v}$ are material constants defined in (3), ρ_m is the mass density of the medium and Ω_e denotes the element e. The damping effect is introduced by Rayleigh's coefficients β and α in mechanical damping matrix $[\mathcal{C}]$.

By assuming that the reluctivity and elasticity are constant along the thickness of the thin magnetostrictive shell layer, it can be incorporated into the simulation using the following submatrices:

$$K_{aa}^{shell} = \delta \nu_{11} \sum_e \int_{L_e} G_a^{shell^T} G_a^{shell} \, dl \tag{13}$$

$$K_{uu}^{shell} = \delta c_{11} \sum_e \int_{L_e} G_u^{shell^T} G_u^{shell} \, dl_e$$

$$K_{ua}^{shell} = \delta \sum_e \int_{L_e} G_u^{shell^T} \mathbb{g}^t G_a^{shell} dl_e$$

$$M^{shell} = \delta \rho_v \sum_e \int_{L_e} N_{ui}^{0\,T} N_{ui}^0 \, dl_e$$

where l_e denotes the line element domain.

The simulation uses the magnetic, electric, and elastic boundary conditions that were employed in the reference [7], [8]. The external boundary of the domain is subject to Dirichlet conditions for the electric scalar potential, while the top and bottom limits are subjected to constant magnetic vector potentials to account for the applied external magnetic field. At the center of the composite, two fixed mechanical displacements are imposed, and the elastic problem is subject to the plane stress condition.

2.4 Nonlinear problem in static regime

A static ME problem is a complex problem that involves the nonlinear ferromagnetic properties of magnetostrictive materials, such as permeability and piezomagnetic coefficients, as well as the linear ferroelectric properties of piezoelectric materials, such as permittivity and piezoelectric coefficients. To simplify this problem, a proposed anhysteretic model for the Ni material is based on the magneto-elastic magnetization $M(H,T)$, which is defined as [13], and the magnetostriction strain $\lambda(H,T)$ is defined in [14]:

$$M(H,T) = \mathrm{M_s}(\coth(z) - \frac{1}{z}) \tag{14}$$

$$\boldsymbol{\lambda}(H,T) = \lambda_s \left(1 - \frac{3 \cdot (\coth(z) - \frac{1}{z})}{z}\right)$$

with $z = \frac{\eta T}{H}$, and where $\mathrm{M_s}$ is the magnetization saturation, H is static magnetic field, T is an applied stress or a residual stress during fabrication process, η is a constant parameter that depends on the magnetic measurement data, and λ_s is the magnetostriction saturation.

Figure 3 illustrates the strong agreement between the results obtained from the proposed model (14) and the magnetic hysteresis measurement of a freestanding nickel film isolated from the Ni/PZT-5H/Ni MEC.

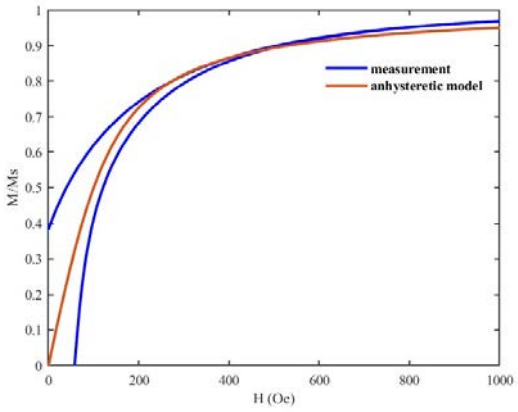

Figure 3: Normalized magnetization curves of the Ni from measurement and the magneto-elastic model

Additionally, Figure 4 displays the piezomagnetic incremental coefficient ${d_{33}}^{H} = \partial_T \boldsymbol{M}(H,T)$, and the relative permeability incremental coefficient ${\mu_{33}}^{T} = \mu_o + \partial_H \boldsymbol{M}(H,T)$ predictions made by the model. Finally, by establishing the piezoelectric tensor $\boldsymbol{d^H}$ with ${d_{33}}^{H}$ and ${d_{15}}^{H} = 3\boldsymbol{\lambda}(H,T)\ /H$ [15], and permeability tensor $\boldsymbol{\mu^T}$, respectively, the tensors $\mathbb{e}$ and $\mathbb{v}^S$ in equation (3) can be obtained using the relations $\mathbb{e} = \boldsymbol{d^H}\ \mathbb{c}^{\boldsymbol{B}}$ and $\mathbb{v}^S = (\boldsymbol{\mu^T} - \boldsymbol{d^H}\mathbb{c}^{\boldsymbol{B}}\boldsymbol{d^{H^T}})^{-1}$.

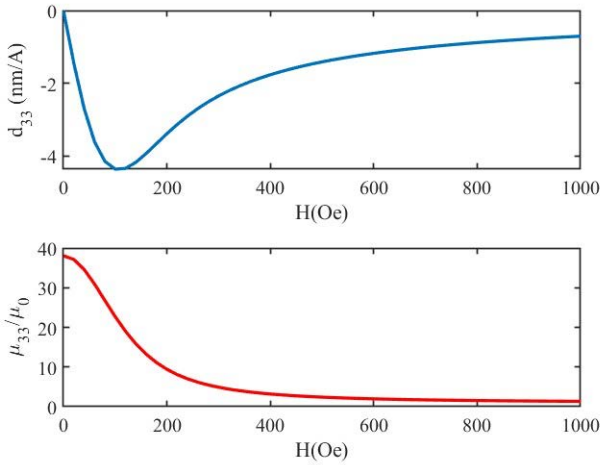

Figure 4: Prediction of piezomagnetic ${d_{33}}^{H}$ and relative permeability ${\mu_{33}}^{T}/\mu_o$ incremental coefficients of the Ni

2.4 Harmonic problem in dynamic regime

The matrix system in harmonic regime is given by (15) [7], [8]:

$$[\mathbb{K}]\{\mathcal{X}\} = \{\mathcal{F}\} \tag{15}$$

with $[\mathbb{K}] = \begin{bmatrix} K_{uu} - \omega^2 M + j\omega C_{uu} & K_{up} & 0 & K_{ua} \\ K_{pu} & K_{pp} & K_{pq} & 0 \\ 0 & K_{qp} & -j\omega Z & 0 \\ K_{au} & 0 & 0 & K_{aa} \end{bmatrix}$

and $\mathcal{X} = [\boldsymbol{u} \quad \boldsymbol{V} \quad Q \quad a_z]^T$, $\mathcal{F} = [0 \quad 0 \quad 0 \quad a_{ex}]^T$

where a_{ex} is the magnetic source of the excitation vector

The circuit equation relative to the influence of the electrical impedance load Z is considered in the global system $[\mathbb{K}]$ with the relation $\{\boldsymbol{V}\}K_{pq} - Zj\omega\{Q\} = 0$, where the electrical charge Q confined to the electrodes is an additional unknown and the incident vector K_{pq} is defined by:

$$K_{pq} = \begin{cases} \pm 1, \text{node} \in \text{electrodes} \\ 0, \text{else where} \end{cases} \tag{16}$$

3 SIMULATION AND MEASUREMENT

The simulations are performed with an applied small signal δH_{ac}= 1 Oe and a resistive load Z=1 MΩ is connected between the Ni films as the electrodes of each MEC, and as shown as Figure 5, our proposed finite element method (FEM) analysis achieved good agreement between the magnetoelectric coefficients obtained in both static and dynamic regimes from the Ni/PZT-5H/Ni MEC experimental measurements and simulation using the piezomagnetic and permeability models presented in Figure 4. However, for the Ni/(YXl)163˚ LiNbO3/Ni MEC, a discrepancy was observed between the simulated and experimental results, which was attributed to the magnetic anisotropy present in their Ni films. To address this, we adapted the parameter η of $\boldsymbol{z}$ in (14) based on magnetic hysteretic measurements and updated the piezomagnetic and permeability from proposed model, accordingly, resulting in improved agreement between simulation and experimental measurements as shown in Figure 6. This magnetic anisotropy issue was attributed to the thermal residual stress generated during the RF sputtering process utilized in the growth of Ni films [16], [17], related to the difference in coefficient of thermal expansion (CTE) presented in Table 1. Additionally, we observed that the remanent ME response α_E for the Ni/PZT-5H/Ni MEC was relatively weak at zero Hdc when compared to the Ni/(YXl)163˚ $LiNbO_3$/Ni composite, where it reached up to 80% of its maximum value. Thus, we concluded that the latter composite can be considered as a self-biased MEC.

Table 1: CTE of the materials in studied MECs

Material	CTE along length direction [K^{-1}]	CTE along width direction [K^{-1}]
Ni	13×10^{-6}	13×10^{-6}
PZT-5H	4×10^{-6}	4×10^{-6}
(YXl)163˚ $LiNbO_3$	15.4×10^{-6}	8.18×10^{-6}

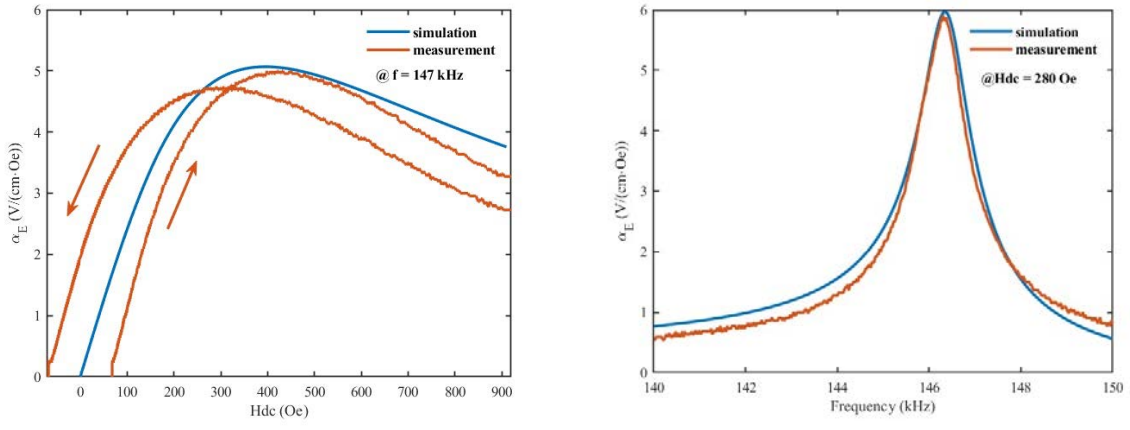

(a) (b)

Figure 5: ME coefficients results in static (a) and dynamic (b) regimes of Ni/PZT-5H/Ni

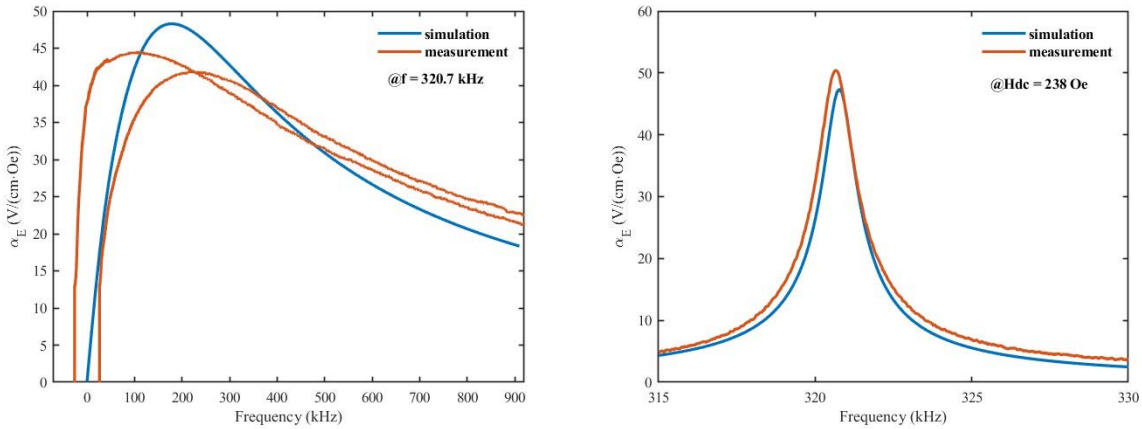

(a) (b)

Figure 6: ME coefficients results in static (a) and dynamic (b) regimes of Ni/(YXl)163˚ $LiNbO_3$/Ni

5 CONCLUSIONS

The article proposes a FEM modeling approach that uses shell elements to simulate thin magnetostrictive layers in ME composites. This method saves considerable computing time compared to the classical approach and has successfully simulated various composites, including Ni/PZT-5H/Ni and Ni/(YXl)163˚ $LiNbO_3$/Ni. The simulated results were in good agreement with experimental measurements, although discrepancies were found in the latter composite due to magnetic anisotropy in the Ni films. By adapting the piezomagnetic and permeability parameters based on magnetic hysteretic measurements, the simulation achieved good agreement. The Ni/(YXl)163˚ $LiNbO_3$/Ni composite exhibited a self-biased characteristic with a significant ME remanent response. In summary, this work provides a valuable tool for exploring the performance of ME composites with thin magnetostrictive layers and can support the development of new ME devices with improved performance.

REFERENCES

[1] S. Kopyl, R. Surmenev, M. Surmeneva, Y. Fetisov, and A. Kholkin, 'Magnetoelectric effect: principles and applications in biology and medicine– a review', *Materials Today Bio*, vol. 12, p. 100149, Sep. 2021, doi: 10.1016/j.mtbio.2021.100149.

[2] C. M. Leung, J. Li, D. Viehland, and X. Zhuang, 'A review on applications of magnetoelectric composites: from heterostructural uncooled magnetic sensors, energy harvesters to highly efficient power converters', *J. Phys. D: Appl. Phys.*, vol. 51, no. 26, p. 263002, Jul. 2018, doi: 10.1088/1361-6463/aac60b.

[3] X. Liang *et al.*, 'A Review of Thin-Film Magnetoelastic Materials for Magnetoelectric Applications', *Sensors*, vol. 20, no. 5, p. 1532, Mar. 2020, doi: 10.3390/s20051532.

[4] Y. Zhou, D. Maurya, Y. Yan, G. Srinivasan, E. Quandt, and S. Priya, 'Self-Biased Magnetoelectric Composites: An Overview and Future Perspectives', *Energy Harvesting and Systems*, vol. 3, no. 1, pp. 1–42, Jan. 2016, doi: 10.1515/ehs-2015-0003.

[5] M. I. Bichurin *et al.*, 'Self-Biased Bidomain LiNbO3/Ni/Metglas Magnetoelectric Current Sensor', *Sensors*, vol. 20, no. 24, p. 7142, Dec. 2020, doi: 10.3390/s20247142.
[6] W. Q. Jing and F. Fang, 'Stress-induced self-biasing of magnetoelectric coupling in embedded Ni/PZT/FeNi composite', *Appl. Phys. Lett.*, vol. 106, no. 21, p. 212901, May 2015, doi: 10.1063/1.4921743.
[7] H. Talleb and Z. Ren, 'Finite element modeling of magnetoelectric laminate composites in considering nonlinear and load effects for energy harvesting', *Journal of Alloys and Compounds*, vol. 615, pp. 65–74, Dec. 2014, doi: 10.1016/j.jallcom.2014.06.121.
[8] H. Talleb and Z. Ren, 'Finite-Element Modeling of a Magnetoelectric Energy Transducer Including the Load Effect', *IEEE Trans. Magn.*, vol. 51, no. 3, pp. 1–5, Mar. 2015, doi: 10.1109/TMAG.2014.2357492.
[9] T. T. Nguyen, F. Bouillault, L. Daniel, and X. Mininger, 'Finite element modeling of magnetic field sensors based on nonlinear magnetoelectric effect', *Journal of Applied Physics*, vol. 109, no. 8, p. 084904, Apr. 2011, doi: 10.1063/1.3553855.
[10] R. C. Kambale, D.-Y. Jeong, and J. Ryu, 'Current Status of Magnetoelectric Composite Thin/Thick Films', *Advances in Condensed Matter Physics*, vol. 2012, pp. 1–15, 2012, doi: 10.1155/2012/824643.
[11] H. Talleb and Z. Ren, 'Mutliphysics Modeling of Thin Layer Magnetoelectric Laminate'.
[12] Zhuoxiang Ren, 'Degenerated Whitney prism elements-general nodal and edge shell elements for field computation in thin structures', *IEEE Trans. Magn.*, vol. 34, no. 5, pp. 2547–2550, Sep. 1998, doi: 10.1109/20.717587.
[13] V. Apicella, C. S. Clemente, D. Davino, and C. Visone, 'Experimental evaluation of external and built-in stress in Galfenol rods', *Physica B: Condensed Matter*, vol. 549, pp. 53–57, Nov. 2018, doi: 10.1016/j.physb.2017.09.081.
[14] H. Talleb and Z. Ren, 'A new nonlinear multiscale magnetostrictive approach for FEM modelling of magnetoelectric composites under magneto-thermo-elastic loading', *Composite Structures*, vol. 303, p. 116260, Jan. 2023, doi: 10.1016/j.compstruct.2022.116260.
[15] M. Hirao and H. Ogi, 'Coupling Mechanism', in *Electromagnetic Acoustic Transducers*, in Springer Series in Measurement Science and Technology. Tokyo: Springer Japan, 2017, pp. 15–38. doi: 10.1007/978-4-431-56036-4_2.
[16] M. Huff, 'Review Paper: Residual Stresses in Deposited Thin-Film Material Layers for Micro- and Nano-Systems Manufacturing', *Micromachines*, vol. 13, no. 12, p. 2084, Nov. 2022, doi: 10.3390/mi13122084.
[17] T. Truong *et al.*, 'Engineering Stress in Thin Films: An Innovative Pathway Toward 3D Micro and Nanosystems', *Small*, p. 2105748, Dec. 2021, doi: 10.1002/smll.202105748.